THE JOURNAL OF PHYSICAL CHEMISTRY C

Article

pubs.acs.org/JPCC

Molecular Transport in Thin Thermoresponsive Poly(*N*-isopropylacrylamide) Brushes with Varying Grafting Density

Teodoro Alonso García,[†] Claudio A. Gervasi,*[,‡,§] María José Rodríguez Presa,[‡] Joseba Irigoyen Otamendi,[†] Sergio E. Moya,[†] and Omar Azzaroni*[,‡]

[†]CIC biomaGUNE, Biosurfaces Unit, Paseo Miramón 182 C, 20009 San Sebastián, Gipuzkoa, Spain

[‡]Instituto de Investigaciones Fisicoquímicas Teóricas y Aplicadas (INIFTA), Facultad de Ciencias Exactas, UNLP, Sucursal 4-C.C. 16, (1900) La Plata, Argentina—CONICET

[§]Laboratorio de Ingeniería de Corrosión y Tecnología Electroquímica, LICTE, Facultad de Ingeniería, UNLP, 1 y 47, (1900) La Plata, Argentina

Supporting Information

ABSTRACT: The effect of the grafting density on the molecular transport through thermoresponsive brushes of poly(*N*-isopropylacrylamide) (PNIPAM) grafted onto flat gold substrates was investigated using voltammetry and impedance spectroscopy. PNIPAM brush layers were synthesized at four different grafting densities using surface-initiated atom transfer radical polymerization (SI-ATRP) from mixed self-assembled monolayers of ω-mercaptoundecyl bromoisobutyrate and undecanethiol chemisorbed on gold surfaces. Tethered PNIPAM layers with grafting densities resulting from initiator concentrations lower than 25% in the thiol monolayer show the same transport properties as the initial self-assembled monolayer before brush synthesis. For higher grafting densities, the diffusion coefficients, D, of the $K_3[Fe(CN)_6]/K_4[Fe(CN)_6]$ redox probe is 7 orders of magnitude smaller than those typically measured in aqueous solutions and independent of whether the brush is collapsed or swollen. The collapse of the PNIPAM brush drives a hydrophilic/hydrophobic transition in addition to structural/conformational transformations of the grafted layers, resulting in still smaller values of D. However, these changes do not lead to a blocking effect on the active area of the gold surface, which is only determined by pinholes or discontinuities in the thiol initiator monolayer. These results are only observed for thin PNIPAM brush layers.

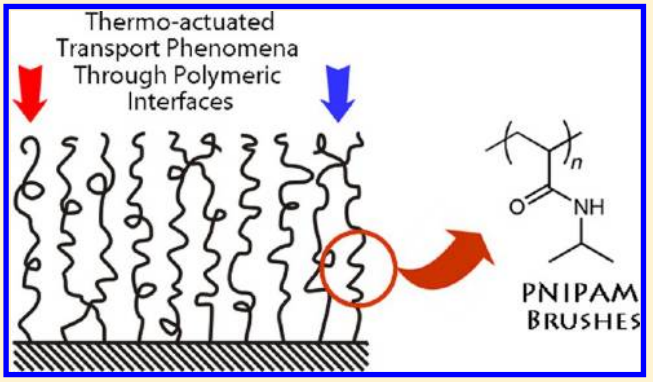

1. INTRODUCTION

Poly(*N*-isopropylacrylamide) (PNIPAM) is the most studied among the thermoresponsive polymers used to obtain brushes that exhibit measurable changes in their thickness with temperature.[1] PNIPAM exhibits phase transition in aqueous environments in a narrow temperature range around 32 °C. Above this temperature, called lower critical solution temperature (LCST), the hydrogen bonding between amide groups of PNIPAM and water molecules is broken and replaced by intramolecular hydrogen bonds between amide groups. As a consequence, the polymer becomes more hydrophobic, excluding water. PNIPAM precipitates in solution above the LCST. In a brush, PNIPAM collapses, reducing thickness besides losing water. These phenomena are reversible. Reducing the temperature below the LCST, the polymer dissolves in water again, and the brush recovers its original thickness.

The actual value of the LCST varies slightly depending on solution conditions, that is, ionic strength, pH, or the configuration of the polymeric system (free, self-assembled, or grafted).[2] In addition, for PNIPAM brushes, the value of the LCST depends on the grafting density and molecular weight of the polymer.[3,4]

The temperature-responsive character of PNIPAM has attracted a lot of attention for the fabrication of "smart" surface modifiers acting like molecular actuators.[5−8]

A clear potential application of PNIPAM brushes is as thermoresponsive barriers. The collapse of PNIPAM above the LCST could generate a hydrophobic layer that restricts transport of water-soluble molecules. Also, the change in thickness of the PNIPAM brush after collapse could increase the volume flow through a pore coated with this polymer as shown by Yameen et al.[9] In this article, swollen PNIPAM brushes below the LCST dramatically decrease ionic transport through nanopores with a reduced effective cross-section.

Even though a great deal of effort has been devoted to characterize the thermoresponsive structural change of PNIPAM

Received: February 18, 2012
Revised: May 25, 2012
Published: June 25, 2012

   dx.doi.org/10.1021/jp301621y | *J. Phys. Chem. C* 2012, 116, 13944−13953

brushes, considerably less effort has been put in the characterization of molecular transport through the brush. Among the scarce work dealing with this subject, it is worth mentioning that by Reuber et al.,[10] where the ionic permeability is studied using cyclic voltammetry on electrodes covered with thick PNIPAM brushes synthesized via electrochemically induced free-radical polymerization. A diffusion coefficient of 10^{-11} cm^2 s^{-1} was calculated for the diffusion of ferricyanide ions across a film of about 100 nm thick.

There is indeed a lack of knowledge of how the architecture of the brush, that is, chain density, chain length, can affect the transport through PNIPAM brushes below and above the LCST. Understanding the transport properties of brushes in relation to their nanoscale organization is extremely important for the design of surfaces and devices with tailored properties as barriers or protecting coatings. Moreover, in the case of PNIPAM, it is not clear how the thermally induced collapse transition affects both molecular transport through the brush and its blocking character of the modified surface, respectively.

To address these issues, we have synthesized thin PNIPAM brushes with varying grafting densities and studied ionic transport through their electrochemical response in presence of a $K_3[Fe(CN)_6]/K_4[Fe(CN)_6]$ redox probe by means of voltammetry and impedance spectroscopy. We aim at measuring the diffusion coefficient of the probe at temperatures below and above the LCST. From the changes in the diffusion coefficient with grafting density and temperature, we intend to evaluate the role on transport of the initiator monolayer and the nanoscale arrangement of the polymer chains in the brush after the collapse.

2. EXPERIMENTAL SECTION

2.1. Chemicals. *N*-Isopropylacrylamide (NIPAM), 2,2′-bipyridine (bpy), copper chloride(I), *N*,*N*′-dimethyl formamide (98%), and blank thiol (1-undecanethiol) were purchased from Sigma-Aldrich (Spain) and used without further purification. Ethanol was purchased form Scharlau S.A. Water purification was performed with a Nanopure purification system. ω-Mercaptoundecyl bromoisobutyrate, the thiol initiator, was synthesized as described elsewhere.[11]

2.2. Sample Preparation. Au substrates were prepared by sputtering deposition, cleaned by sonication, followed by water rinsing, while the final cleaning step comprised exposure to UV radiation in a Bioforce Nanosciences chamber for 30 min just before modification step. Modification of Au surfaces was carried out by immersion in 10 mM thiol solutions in ethanol for 16 h to allow the spontaneous formation of the initial assembled monolayer (SAM). To obtain brushes with four different grafting densities, four different thiol solutions were prepared by mixing initiator and inhibitor thiols with the following content of the initiator: 100, 50, 25, and 5%.

Polymer brushes were grown from the different mixed SAMs constituted of ω-mercaptoundecyl bromoisobutyrate (thiol initiator) and 1-undecanethiol (blank thiol) chemisorbed on gold, which ultimately defines the grafting density of the polymer chains. Polymer synthesis was accomplished by surface-initiated aqueous atom transfer radical polymerization (SI-ATRP).[12,13]

Polymer brushes were prepared as follows: thiol-functionalized surfaces were immersed in a mix of CuCl/Bipyridine/monomer in a ratio of 1:2:10 in DMF/water (3:2) as the solvent, at 40 °C in an inert atmosphere of N_2. The polymerization was left to proceed for 5 h. At the end, the subtrates were rinsed with water, acetone, ethanol, and water.

2.3. Experimental Techniques. Ellipsometric thickness determinations were performed with a spectroscopic rotating compensator ellipsometer (M2000 V, Woollam, NE). Ellipsometric data, Δ and ψ, were acquired simultaneously, over a wavelength range from λ = 380 to 1000 nm, at an angle of incidence of 65° and with a time resolution of 5 s. The working temperature was 20 °C for dry film conditions, while thicknesses were also determined at 20 and 40 °C in KCl in a custom-built fluid cell (Q-Sense, Vastra Frolunda, Sweden) with a total volumen of ∼300 μL. Reported thickness values result from an average over three measurements at different spots on the PNIPAM brush surfaces.

Atomic force microscopy analysis was measured with a Veeco Multimode atomic force microscope connected to a Nanoscope V controller, and the films were imaged in Tapping mode (polymer brushes) and in contact mode (initial thiol SAMs) in a closed fluid cell. Silicon nitride cantilevers (DNPS, K = 0.32 N m^{-1}) were available from Bruker.

Electrochemical measurements were carried out at room temperature in a conventional three-electrode cell. A large area platinum sheet was used as the counter electrode, and a saturated calomel electrode (SCE) served as the reference electrode. All potentials in the text and figures are referred to the SCE. As working electrodes, we used the modified Au substrates coated with the initial thiol monolayer or PNIPAM brushes grown on top of the mixed reactive thiol monolayer.

Solutions of 0.1 M KCl were used as supporting electrolytes and prepared from analytical grade (Merck) reagents and Milli-Q water. Before performing each measurement, the working electrode was thoroughly rinsed with Milli-Q water and immersed in the supporting electrolyte solution for 10 min. Experiments were performed under purified N_2 gas saturation at 20 and 40 °C in the presence of a 1 mM $K_3[Fe(CN)_6]/K_4[Fe(CN)_6]$ (1:1) mixture as a redox probe in the supporting electrolyte.

Cyclic voltammetry measurements were performed by scanning the potential in the window where oxidation and reduction of the redox couple take place at a scan rate of 50 mV s^{-1}.

Impedance spectra were obtained with a Zahner IM6d electrochemical workstation on modified working electrodes with 0.50 cm^2 apparent area. The dc potential was held at the open circuit potential, while a 10 mV amplitude AC voltage was applied.

The measuring frequency f used for EIS measurements ranged from 100 kHz to 1 mHz. Impedance data analysis was performed according to proper transfer function derivation and identification procedures, which involved complex nonlinear least-squares (CNLS) fitting based on the Marquardt−Levenberg algorithm.[14]

3. RESULTS AND DISCUSSION

The mixed initial SAM, graphically outlined in Figure 1, provides initiating sites for brush growth as well as a barrier of hydrophobic molecules between the electrode surface and the hydrophilic electroactive species in the electrolyte.[15] Moreover, as is well-known, most SAMs contain a certain density of defects or pinholes, at which electron transfer reactions between electroactive molecules and the electrode surface may take place with considerably less hindrance. If the pinhole density is large enough, currents due to electron tunneling through the blocking layer become negligible.[16] Furthermore, for impedance experiments recorded at the open circuit potential where a very low overpotential (essentially the amplitude of the AC voltage) is

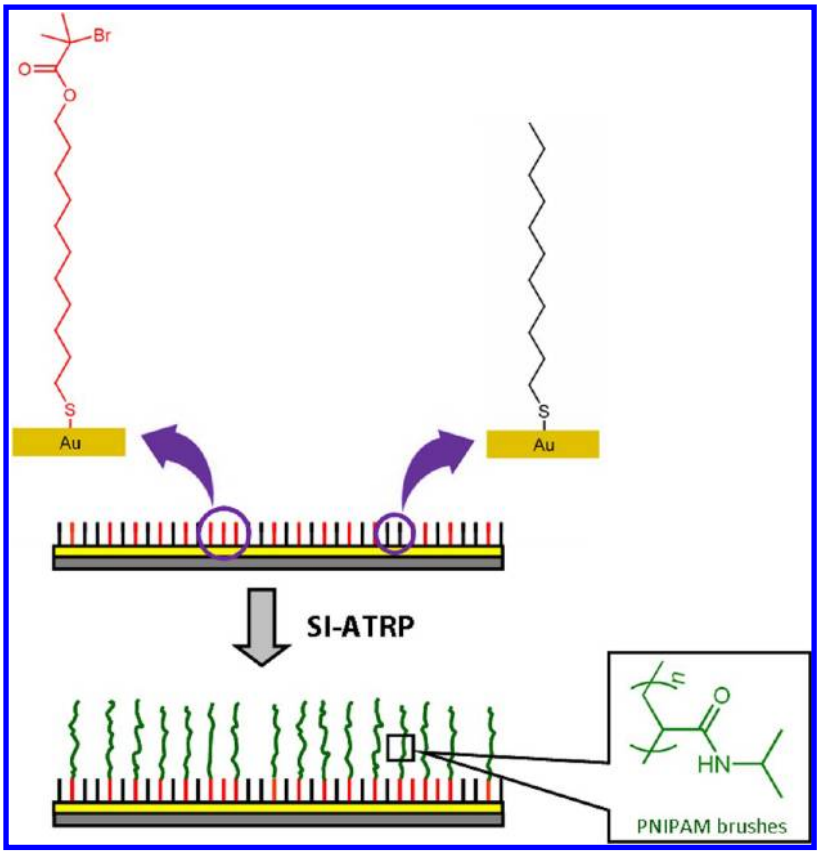

Figure 1. Schematic representation of a Au substrate modified with an initial SAM containing a mixture of initiator/inhibitor thiols (upper sketch) and the resulting surface after growth of a PNIPAM brush via ATRP (lower sketch).

applied, tunneling currents are anticipated to have a minimal effect on the pinhole currents.[17] Under these conditions, the electrochemically active area of the substrate corresponds to the fractional area determined solely by pinhole sites and other defects in the initial SAM. In the case studied here, the fractional area of pinholes may be affected by the collapse of the brush with the temperature, which could block the surface. The concept of fractional coverage is essential for the interpretation of voltammetric and impedance data obtained with SAM-coated electrodes.[18] Clearly, the best way to estimate the fractional coverage is to measure the charge-transfer resistance in the presence of the SAM/brush system and compare these values with those for an electrode that is unmodified.

We will first consider the voltammetric response of the SAM/brush-coated electrodes. In Figure 2, we observe the effect of switching the electrolyte temperature T from a value below the LCST to a value above the LCST on the voltammetric response of an electrode modified with a PNIPAM brush grown from an initial SAM containing 25% thiol initiator. The separation of peak potentials was 75 mV at 40 °C. These data for a Au electrode are consistent with a quasi-reversible electron transfer model. When a bare gold electrode is modified with a SAM, a noticeable decrease in the peak current is observed in the cyclic voltammogram as well as an increase in the splitting of the peak potentials and a tendency of the voltammogram to adopt a sigmoidal line shape. These observations are in agreement with those obtained for ultramicroelectrodes and indicate that the electron transfer reaction might be occurring at pinhole sites.[19] Higher peak current densities and a smaller peak separation were obtained as the measuring temperature is increased. This response can

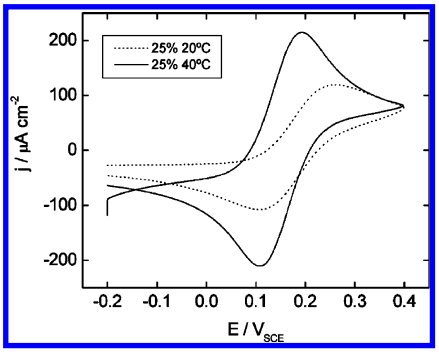

Figure 2. Cyclic voltammograms for a single electrode modified with a PNIPAM brush grown from an initial SAM containing 25% thiol initiator. Voltammograms were recorded at a sweeping rate of 50 mV s^{-1} and at two electrolyte temperatures 20 (···) and 40 °C (—).

be interpreted in terms of faster electrochemical kinetics exhibited by the couple for higher temperature values.

At this point, it is probably worth mentioning briefly that for quasi-reversible electrode reactions[20] (i) a decrease in the diffusion coefficient D reduces the shift in the peak potentials E_p away from the formal potential of the electrode and (ii) the same effect is also obtained with an increase in T. However, in this system, an increase in T leading to a collapsed brush is expected to reduce D; hence, it is not possible from the voltammetric results to uncouple both effects. Consequently, the observed changes of the voltammetric responses shown in Figure 2 can not be solely ascribed to a marked reduction of D related to a collapsed brush but also to considerably more facile

dx.doi.org/10.1021/jp301621y | J. Phys. Chem. C 2012, 116, 13944−13953

kinetics of the heterogeneous electron transfer reactions after increasing T.

In Figure 3, we observe the voltammetric responses of the electrodes coated with PNIPAM synthetized from a SAM with

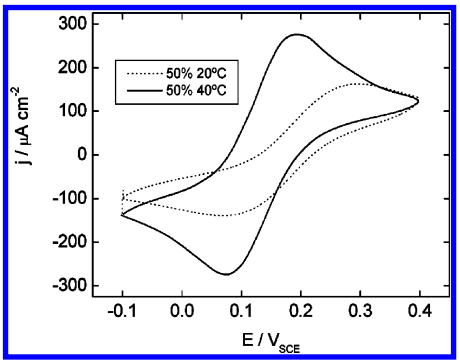

Figure 3. Cyclic voltammograms for a single electrode modified with a PNIPAM brush grown from an initial SAM containing 50% thiol initiator. Voltammograms were recorded at a sweeping rate of 50 mV s^{-1} and at two electrolyte temperatures 20 (···) and 40 °C (—).

50% thiol initiator and recorded at 20 and 40 °C. Current densities j in both Figures 2 and 3 were calculated relative to the apparent electrode area, which precludes a direct comparison of absolute j values between these two figures, unless the real active areas are known. Figure 3 shows a similar behavior as Figure 2.

These results differ strongly from those obtained for thick PNIPAM brushes where the redox probe exhibits a quasi-reversible wave at 25 °C, that is, for the swollen, extended conformation of the polymer brush, while the redox voltammetric response becomes almost undetectable after raising the temperature to 45 °C. In this case, results are explained in terms of a brush in a collapsed state hindering charge transfer between the redox probe and the electrode surface.[21] On the other hand, Reuber et al.[10] claim that the voltammetric response of ferricyanide ions on electrodes covered with a thick PNIPAM hydrogel arises from the hindered diffusion of the electroactive ions between the bulk electrolyte and the collapsed film.

Figure 4 shows voltammetric responses for an electrode modified with an initial SAM containing 100% thiol initiator and for a second electrode modified with an initial SAM con-

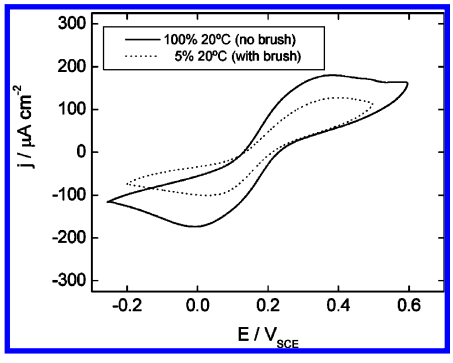

Figure 4. Cyclic voltammograms for an electrode modified with an initial SAM containing 100% thiol initiator (—) and for a second electrode modified with an initial SAM containing 5% thiol initiator from which the PNIPAM brush was grown (···). Voltammograms were recorded at a sweeping rate of 50 mV s^{-1} and at 20 °C.

taining 5% thiol initiator from which the PNIPAM brush was grown. Because the resulting real active area after covering the electrode with the initial SAM varies from sample to sample, no comparison can be made between the absolute values for the peak current densities in Figure 4 that were calculated relative to the electrode's geometric area. In both cyclic voltammograms, an increase in the splitting of the peak potentials relative to the expected value for a bare Au electrode can be clearly observed as well as a tendency of the voltammograms to adopt a sigmoidal shape that is in agreement with the results also measured at 20 °C and discussed above. Moreover, the separation of peak potentials is practically the same for both electrodes. This behavior can be interpreted as resulting from the presence of the initial SAM alone, independent of the presence of the brush. Such a brush grown with low grafting density proves unable to affect the diffusion coefficient in the system. It is worth emphasizing here that D at the electrode without a grown brush corresponds to the ionic species in solution, and consequently, it is much larger than that expected for diffusion through the polymer film. On the basis of theoretical postulates and numerical simulations, it has been claimed that brushes of low grafting density may display a lateral "phase separation", with grafted chains forming isolated clusters with free space among them.[2] To either confirm or rule out a possible phase separation effect in the initial SAMs formulated with two different thiols, AFM images were obtained of the initiating layers by a phase-sensitive technique such as AFM in lateral force mode. Results for a SAM obtained with 5% thiol initiator and a SAM with a 100% inert thiol are shown in Figure S1 in the Supporting Information. Comparison of AFM friction images reveals the same overall morphology for both samples and the absence of phase-separated nanometer scale domains in the mixed SAM.

For an initial mixed SAM without phase-segregated domains, inhomogeneous coverage by the brush chains along the SAM surface would result in semi-infinite diffusion conditions for the redox probe at the electrode. Thus, at low grafting density, that is , if the distance between two neighboring polymer chains is greater than the radius of gyration of free polymer chains, two tethered chains feel no interaction, and two conformations of polymers end-attached to a surface are possible, described in the literature as "mushroom-like" and "pancake-like". If polymer chains are well soluble in the solvent, they form a "mushroom" structure that might explain similar results presented in Figure 4 for both samples. Indeed, probe microscopy imaging of the brush grown from an initial SAM containing 5% thiol initiator displays randomly distributed patches of uncovered surface as inferred from phase-contrast imaging in tapping mode AFM (Figure 5). These uncovered domains are absent in AFM images obtained from the brush grown from an initial SAM containing 100% thiol initiator (Figure 6).[22]

To gain a deeper insight into the transport through PNIPAM and the possible blocking effect of collapsed PNIPAM layers, we performed impedance experiments. Figure 7 shows impedance spectra for an electrode modified with an initial SAM containing 100% thiol initiator without subsequent brush growth. Nyquist diagrams in Figure 7a exhibit a semicircle in the high frequencies f region followed by a straight line with slope approaching −45° at low frequencies. The semicircle is related to electron transfer-limited processes at the uncovered gold surface, whereas the straight line is compatible with semi-infinite linear diffusion

dx.doi.org/10.1021/jp301621y | J. Phys. Chem. C 2012, 116, 13944−13953

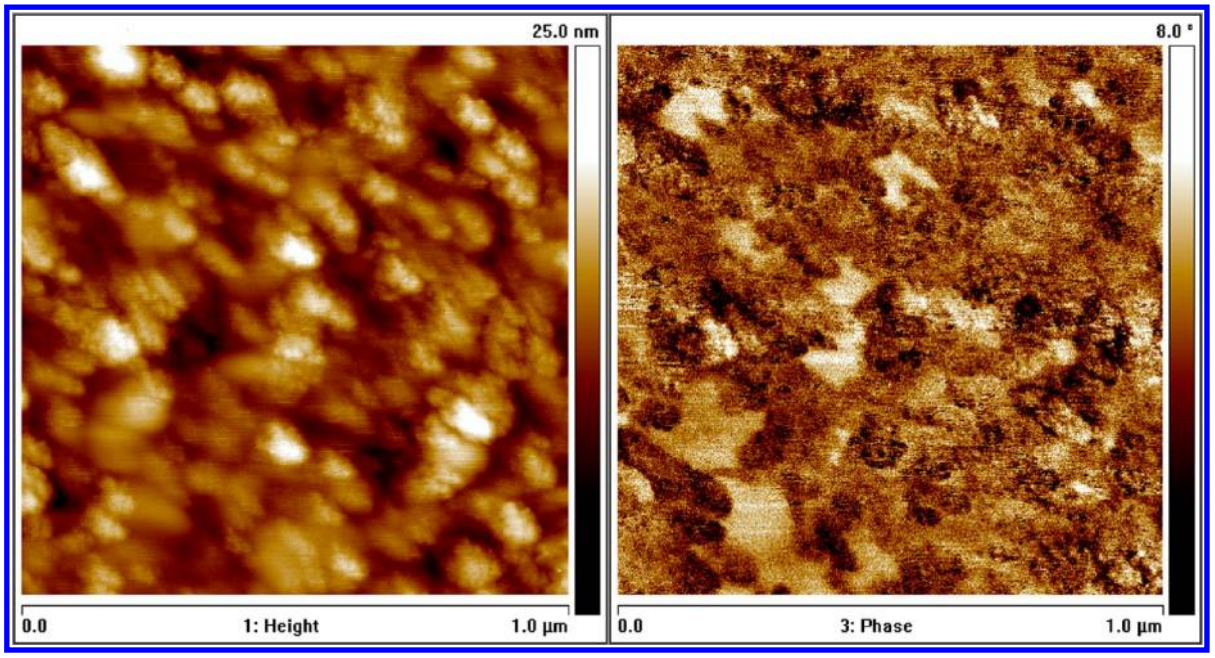

Figure 5. AFM topographic images of the brush grown from an initial SAM containing 5% thiol initiator; image contrast in terms of height and phase.

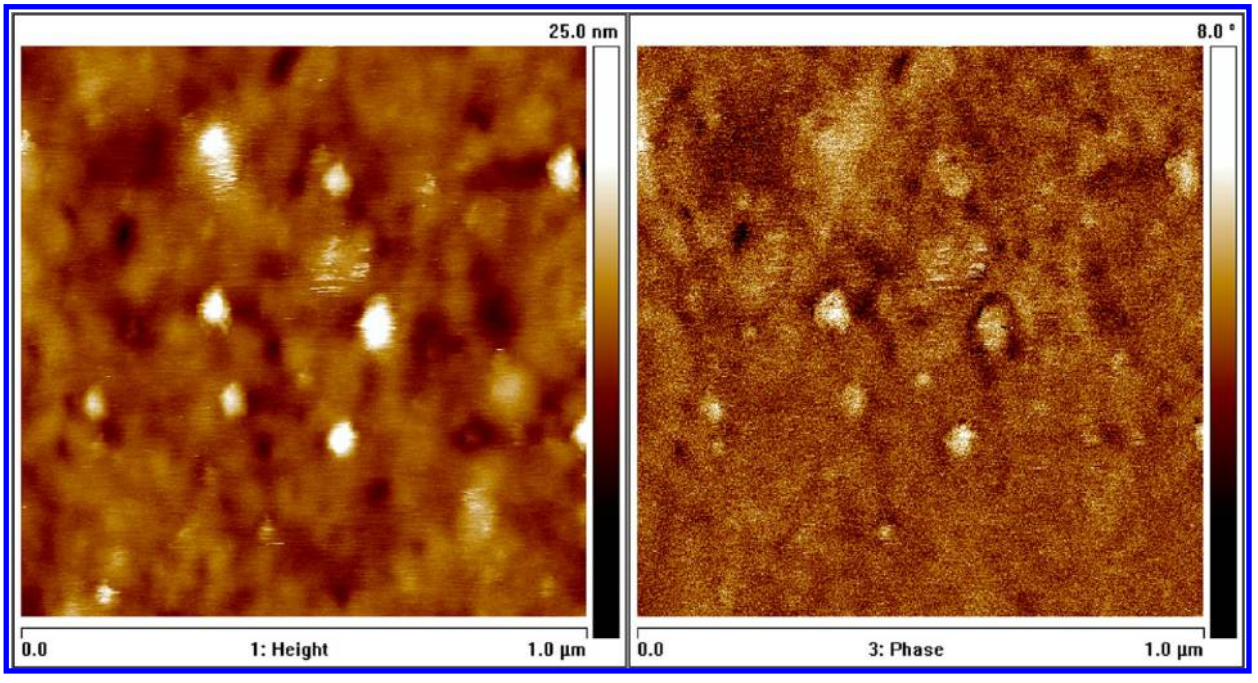

Figure 6. AFM topographic images of the brush grown from an initial SAM containing 100% thiol initiator; image contrast in terms of height and phase.

or Warburg diffusion of the redox probe in the electrolyte. Hence, the electron transfer kinetics and the diffusional characteristics can be extracted from the EIS data. The semicircle diameter represents the charge transfer resistance R_{ct}, whereas the intercept of the semicircle with the real part of the impedance Re(Z)-axis for $f \rightarrow \infty$ corresponds to the solution resistance, R_s. Measured impedance data were corrected by the apparent electrode area. Data representation in terms of Bode plots is also included in Figure 7b since they show the frequency response characteristic of the system over the entire measured frequency range, with points equally spaced in the frequency axis.

The same qualitative behavior was measured for an electrode modified with an initial SAM containing 5% thiol initiator from which the PNIPAM brush was grown (Figure 8). A comparison between the dynamic behavior in the low frequency regions shown in Figures 7 and 8 indicates that for low grafting densities, resulting, for example, from an initiator concentration of 5% in the initial SAM, the polymer brush is incapable of affecting the transport properties in the system. This observation

dx.doi.org/10.1021/jp301621y | J. Phys. Chem. C 2012, 116, 13944−13953

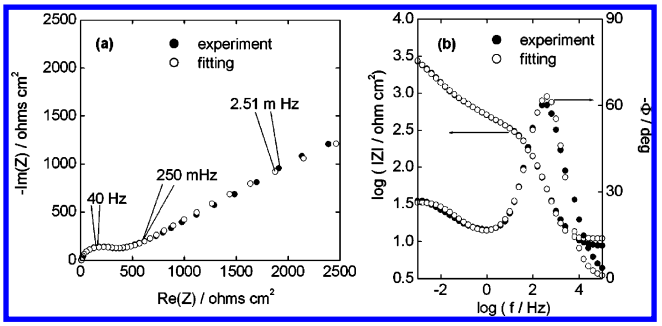

Figure 7. Impedance spectra for an electrode modified with an initial SAM containing 100% thiol initiator without subsequent brush growth. Measured and fitted data represented as Nyquist diagrams (a) and Bode plots (b). Experimental data (●) and fit results (○) according to the equivalent circuit (Figure 11a) and the reaction impedance Z_f from eq 7.

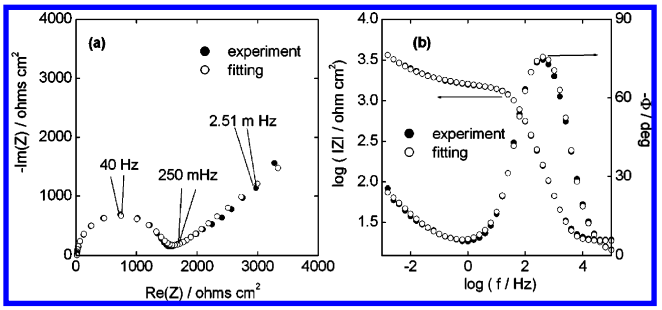

Figure 8. Impedance spectra for an electrode modified with an initial SAM containing 5% thiol initiator from which the PNIPAM brush was grown. Measured and fitted data represented as Nyquist diagrams (a) and Bode plots (b). Experimental data (●) and fit results (○) according to the equivalent circuit (Figure 11a) and the reaction impedance Z_f from eq 7.

is in agreement with the corresponding information derived from voltammetric data.

Impedance spectra were measured at 20 and 40 °C for an electrode modified with an initial SAM containing 50% thiol initiator from which the PNIPAM brush was grown. Experimental data and fitting results are presented in Figures 9 and 10, respectively.

Similarly to the impedance data discussed before, the high frequency region of Nyquist spectra in Figures 9 and 10 is characterized by a semicircle related to the electron transfer reactions at the uncovered gold surface. However, the main difference with data in Figures 7 and 8 is associated with the low frequency region containing diffusion effects that are now compatible with finite-length diffusion type impedances. It is only quite recently that it has become clear that this type of behavior can be observed for electrodes modified with PMETAC polymer brushes.[23] For this purpose, it has been shown that impedance spectra should be recorded over as wide a range of frequency as possible before any attempt is made to interpret the data.[24]

The same qualitative behavior was observed for each electrode modified with an initial SAM containing a percentage of thiol initiator larger than 5% and from which the PNIPAM brush was grown (data not shown).

Because both sets of data (Figures 9 and 10) were obtained from the same electrode, it is possible here to compare the absolute values of the measured impedance between the two experiments. Clearly, charge transfer resistance R_{tc} becomes smaller as the temperature is raised from 20 to 40 °C, but the resistive term of the diffusional impedance at low frequencies R_d remains practically unaltered. Bearing in mind that each impedance value is inversely proportional to the electroactive area, we can conclude that by switching the temperature from 20 to 40 °C, the active area of electrode is not affected, but the charge transfer at the surface becomes faster. An additional indication that the charge transfer process becomes faster is given by a change in the frequency range for which the corresponding semicircle in the Nyquist plots is detected. For example, at 20 °C, the experimental point measured at 40 Hz barely exceeds the semicircle's maximum, while at 40 °C, the same point is measured when the high frequency semicircle has been completely measured (see Figures 9a and 10a).

Dynamic behavior related to diffusion effects can be preliminarily analyzed, on a qualitative basis, also by comparison of the spectra shown in Figures 9 and 10. Thus, the characteristic frequency value f_{char} of the inflection point at which the diffusional part of the impedance departures from the linear Warburg behavior and starts to describe a concave downward arch reaching the Re(Z)-axis increases with an increase in the diffusion coefficient D and decreases as the diffusion path length δ augments. Assuming that δ is the thickness of the polymer brush, as explained below, it is expected that the thermally collapsed brush (40 °C) be associated with a higher f_{char} due to a thinner diffusion path or with a lower f_{char} if the major effect is to reduce D. In this case, $f_{char} \approx 15$ mHz for both experiments in Figures 9 and 10. Consequently, the expected decrease in δ values due to the polymer brush collapse must be compensated for by a decrease in D, thus leaving f_{char} nearly invariant.

It has been shown in the previous qualitative discussion of impedance data that the technique allows separating the individual effects of the thermally induced collapse transition on both the molecular transport through the brush and the blocking

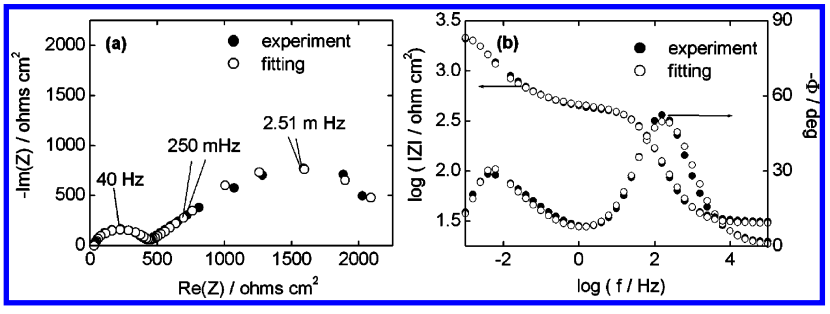

Figure 9. Impedance spectra recorded at 20 °C for an electrode modified with an initial SAM containing 50% thiol initiator from which the PNIPAM brush was grown. Experimental data (●) and fit results (○) according to the equivalent circuit (b) and the reaction impedance Z_f from eq 6.

dx.doi.org/10.1021/jp301621y | J. Phys. Chem. C 2012, 116, 13944−13953

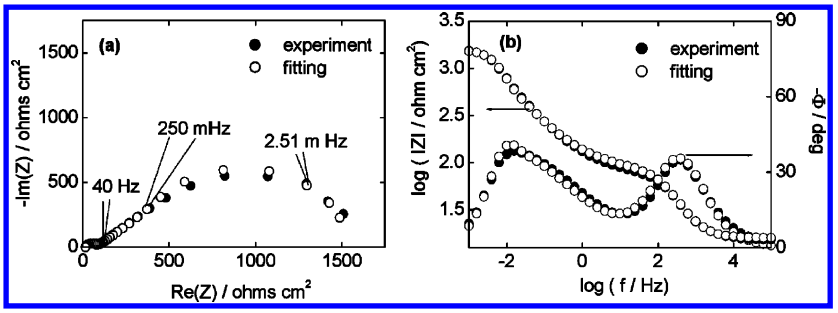

Figure 10. Impedance spectra recorded at 40 °C for an electrode modified with an initial SAM containing 50% thiol initiator from which the PNIPAM brush was grown. Experimental data (●) and fit results (○) according to the equivalent circuit (Figure 9b) and the reaction impedance Z_f from eq 6.

character of the modified surface, respectively. However, the points made require confirmation through a quantitative analysis of impedance data.

As previously pointed out, the impedance response of the system can be described in terms of a partially blocked electrode surface determined by the initial SAM. Then, the main influence of the polymer brush would be to slow down the mass transfer rate of the redox probe. A physical model of the interface of the modified electrode is suggested on the basis of the equivalent circuit for the impedance in Figure 11a, with R_e

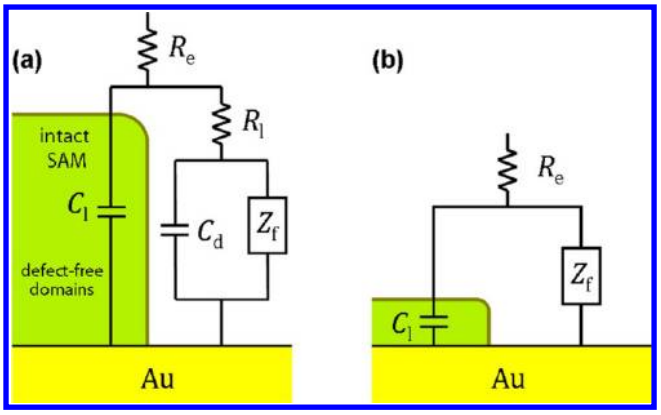

Figure 11. Schematic representation of an electrode modified with a SAM from which the PNIPAM brushes were grown. The SAM contains defects exposing the bare Au surface. The corresponding equivalent circuit is presented in its general form (a) and in a simplified form (b).

the electrolyte resistance, C_{dl} the double layer capacitance, R_l the resistance of the ionic path within the brush, C_l the capacitance of the intact SAM, and Z_f the Faradaic impedance associated with the electrochemical reactions of the redox probe at the fraction of area of the electrode that is not blocked, that is, at the defect sites of the initial SAM.

The equivalent circuit in Figure 11b is a simplification of that in Figure 11a and corresponds to a condition prevailing in many of our experiments, where R_l is negligible and C_l is considerably larger than C_{dl}.

Theoretical derivation of the interfacial impedance Z_f requires the following assumptions that are partially supported by the voltammetric analysis and the qualitative aspects of the experimental impedance, as presented above.

As a first approximation, partial coverage θ does not affect significantly linear conditions for the mass-transport step at a planar electrode; the effect of the partial coverage is simply to reduce the active area. All impedances, with the exception of the electrolyte resistance R_e and the capacitive reactance related to C_l, are inversely proportional to the active area; thus, Z_f is inversely proportional to the fractional area of active surface $(1 - \theta)$. The brush layer represents a diffusion-limiting barrier of finite thickness δ for electroactive molecular probes. In this way, the electrode is uniformly accessible to mass transfer through a hydrated brush of finite thickness. The diffusion impedance response of the brush-covered electrode, when the resistance of the brush to diffusion is much larger than that of the bulk electrolyte, can be approximated by the diffusion impedance of the brush alone.

The electrochemical reaction can formally be written as

$$\mathrm{O} + \mathrm{e} \underset{k_a}{\overset{k_c}{\rightleftarrows}} \mathrm{R} \tag{1}$$

where O is the oxidized species $[Fe(CN_6)]^{3-}$ and R represents the reduced species $[Fe(CN)_6]^{4-}$.

The potential (V) dependence of the rate constants can be expressed by an exponential law:

$$k_a = k_a^o \exp[b_a(V - V_r)] \tag{2}$$

$$k_c = k_c^o \exp[b_c(V - V_r)] \tag{3}$$

where $b_c = -\alpha_c F/RT$ and $b_a = \alpha_a F/RT$, k^o is a constant independent of V, α is the transfer coefficient and V_r the Nernst equilibrium potential.

Charge balance is given by:

$$I_f = -A_e F[k_c C_O(0) - k_a C_R(0)] \tag{4}$$

where $C_O(0)$ and $C_R(0)$ represent concentrations of the oxidized and reduced species at the surface and A_e is the active electrode area. The negative sign arises from the assumed convention in which the cathodic current is negative. For simplicity, we assume $D_O = D_R = D$.

Consequently, the reaction impedance can be identified as

$$Z_f = R_{ct} + R_{ct}\frac{(k_c - k_a)}{D\sqrt{\frac{j\omega}{D}}}\tanh\left(\delta\sqrt{\frac{j\omega}{D}}\right) \tag{5}$$

which, after rearranging, reduces to

$$Z_f = R_{ct} + \frac{\sigma}{\sqrt{\omega}}[\tanh(B\sqrt{j\omega})](1 - j) \tag{6}$$

where $j = (-1)^{1/2}$, $\omega = 2\pi f$, is the angular frequency of the potential perturbation, and the so-called mass transfer coefficient σ contains the contributions of the forms O and R

dx.doi.org/10.1021/jp301621y | J. Phys. Chem. C 2012, 116, 13944−13953

Table 1. Best-Fitting Parameters Obtained for the Experimental Spectra Shown in Figures 5 and 6 and Spectra Recorded with the Same Electrodes but at 40° C[a]

% init/T (°C)	R_e (Ω cm^2)	C_l (F cm^{-2})	R_l (Ω cm^2)	C_{dl} (F cm^{-2})	R_{ct} (Ω cm^2)	σ (Ω cm^2 s$^{-1/2}$)
5/20	18.88	1.18×10^{-4}	<0.1	2.4×10^{-6}	2000	0.0033
5/40	13.53	5.68×10^{-5}	<0.1	2.2×10^{-6}	595	0.0052
100% no brush/20	11	8.2×10^{-4}	<0.1	7.6×10^{-6}	1118	0.00154
100% no brush/40	12.14	6.7×10^{-4}	<0.1	8.7×10^{-6}	491	0.00524

[a]Data fitted to the theoretical impedance resulting from the equivalent circuit (Figure 11a) and the reaction impedance Z_f according to eq 7.

Table 2. Best-Fitting Parameters Obtained from the Fitting of the Experimental Spectra Shown in Figures 9 and 10 and Spectra Recorded with the Electrodes Where Brushes Were Grown from Initial SAMs Containing 25 and 100% Thiol Initiator at 20 and 40° C[a]

% init/T (°C)	R_e (Ω cm^2)	C_l (F cm^{-2})	R_{ct} (Ω cm^2)	B (s$^{1/2}$)	wet δ (nm)	$D \times 10^{13}$ (cm^2 s^{-1})
100/20	42	6.26×10^{-6}	7650	5.62	38 ± 5.1	4.65 ± 1.2
100/40	27.57	1.51×10^{-5}	286	6.72	21 ± 2.5	0.99 ± 0.23
50/20	30.14	2.19×10^{-5}	392	11.83	40 ± 2.1	1.16 ± 0.12
50/40	16	4.4×10^{-5}	71.05	8.8	17 ± 1.0	0.37 ± 0.05
25/20	26.6	2.05×10^{-5}	498	6.64	39 ± 0.9	3.45 ± 0.16
25/40	26.58	2.77×10^{-5}	66	6.52	19 ± 0.4	0.85 ± 0.03

[a]Impedance data were fitted to the theoretical impedance derived from the equivalent circuit (Figure 11b) and the reaction impedance Z_f according to eq 6. Measured values for the brush wet thickness δ and calculated values for the diffusion coefficient D of the redox probe.

and $B = \delta/\sqrt{D}$. The complete mathematical treatment used to derive eq 6 can be found elsewhere.[23,24]

However, when the polymer brush is absent or it has been grown with a very low grafting density, for example, 5% content of thiol initiator in the initial SAM, δ corresponds to the diffusion length in the electrolyte solution. More specifically, δ becomes infinitely large, and the conditions correspond to those of semi-inifinite linear diffusion that is described by a Warburg impedance. Because tanh (x) tends asymptotically to the value 1 as x tends to infinity,[25] eq 6 reduces to

$$Z_f = R_{ct} + \frac{\sigma}{\sqrt{\omega}}(1 - j) \tag{7}$$

Experimental impedance spectra in Figures 7 and 8 together with spectra recorded with the same electrodes but at 40 °C were fitted to a model comprising the equivalent circuit in Figure 11a and the expression for Z_f from eq 7. Fit results are also included in Figures 7 and 8 together with the corresponding experimental data. A very good agreement between theory and experiment can be observed. Best-fitting parameters are assembled in Table 1.

During the fitting process, all parameters were allowed to vary freely until they reached their optimized values. As indicated in the qualitative analysis, R_{ct} values are smaller at 40 °C, that is, in conditions of thermally induced collapse of PNIPAM brushes. Moreover, the ratio of R_{ct} values measured at 20 and 40 °C is nearly the same for the electrode covered only with the initial SAM (100% initiator), and the electrode covered by the initial SAM (5% initiator) from which a brush was grown with very low grafting density. The same is true for the ratio of the Warburg coefficients. These facts confirm that the effect of changing T is restricted to the electrochemical kinetics and that the polymer brush grafted from a SAM with very low initiator concentration (5% in the initial SAM) does not set up a diffusion barrier for the redox probe.

A charge transfer resistance $R_{Ct}^{\text{bare Au}} = 24.43$ Ω cm^{-2} for a Au(111) surface in 0.01 M $HClO_4$ at 25 °C was measured by Janek and Fawcett,[18] which we use to make a rough estimation of the apparent fractional electrode coverage θ in our experiments. Thus, we can write

$$\theta = \left(1 - \frac{R_{ct}^{\text{bare Au}}}{R_{ct}^{\text{initial SAM}}}\right) \tag{8}$$

where $R_{Ct}^{\text{initial SAM}}$ corresponds to the charge transfer resistance measured at 20 °C for the electrodes modified with (i) an initial SAM containing 5% thiol initiator from which the PNIPAM brushes were grown and (ii) an initial SAM containing 100% thiol initiator without subsequent brush growth. These values are shown in Table 1. In spite of some differences with the experiments in the work from the literature taken as reference, like, for example, electrolyte T and composition, θ results 0.988 and 0.978, respectively, which are in good agreement with those calculated for the following comparable electrodes: Au(111) modified with decanethiol (DT) and Au(111) modified with ω-hydroxydecanethiol (HDT).[18] This fact, in turn, can be taken as a validation of the theoretical model used in this work.

Experimental impedance spectra in Figures 9 and 10 together with spectra recorded with the electrodes, where the brushes were grown from an initial SAM containing 25 and 100% thiol initiator at 20 and 40 °C (impedance data not shown), were fitted to a model comprising the equivalent circuit depicted in Figure 11b and the expression for Z_f from eq 6. Fit results are also included in Figures 9 and 10 together with the corresponding experimental data. A very good agreement between theory and experiment can be observed. Best-fitting parameters are assembled in Table 2.

As before, R_{ct} values are smaller at 40 °C, that is, under conditions of thermally induced collapse of PNIPAM brushes and in agreement with an activated process. Consequently, for all studied grafting densities of thin grafted PNIPAM brushes, increasing T above LCST results in faster electrochemical kinetics without detectable changes in the electrodes' surface coverage.

Using fit parameter B in Table 2, we can derive the diffusion coefficient D of the electroactive molecule, independent of the actual value for the active area of the electrode or the need to

dx.doi.org/10.1021/jp301621y | J. Phys. Chem. C 2012, 116, 13944−13953

derive A_e from a different source, when it is different from the electrode's geometric area, like in the present system. Independent calculations of D cannot be made from voltammetric results or results obtained with another electroanalytical technique, because A_e and D are always part of the same fitting parameter in the corresponding theoretical equations. Generally speaking, electrochemical techniques are best suited for studying mass transport processes through thin polymer films. However, for the present study, the possibility of obtaining a parameter like B that is independent of A_e, represents a considerable advantage of impedance spectroscopy over other electrochemical techniques.

To estimate D, we need to consider the brush thickness δ under the different working conditions. Thicknesses of polymer brushes as measured in the dry state with ellipsometry are shown in Figure 12.

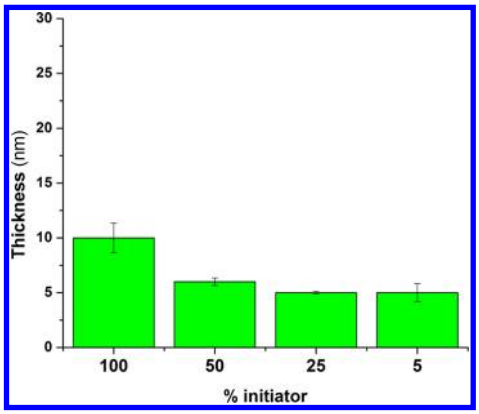

Figure 12. Ellipsometric thicknesses of PNIPAM brushes grown from thiol monolayers with different percentages of initiator as measured in the dry state.

The following swelling factors according to the grafting density, whether high (HD), medium (MD), or low (LD), were obtained after measuring wet thickness values at 20 °C: 3.8 (HD for 100% initiator), 6.7 (MD for 50% initiator), and 7.8 (LD for 25% initiator). These factors are in good agreement with comparable literature data.[26] Finally, considering the measured wet thickness values at 40 °C, the following relationship[27] was confirmed to be valid for the change in thickness of PNIPAM brushes due to the thermally induced collapse

$$\delta_{wet}^{20^\circ C} = 2\delta_{wet}^{40^\circ C} \quad (9)$$

The measured values of δ_{wet} and the calculated values for D are assembled in Table 2. It can be clearly observed that D values for the redox molecule in the brush are much smaller than the corresponding value in an aqueous electrolyte and similar to those obtained in thick surface-attached PNIPAM gel layers[10] or in comparable grafted PMETAC brushes.[23,24] Finally, comparing D values measured below LCST and above that temperature, at each grafting density, an additional hindrance to diffusion associated with the brush collapse can be observed. For all studied grafting densities, D results ca. four times smaller above LCST, which is compatible with a decrease in wet δ of two times to leave f_{char} practically invariant, as indicated above. Accordingly, derived values of D match exactly the proportionality existing between f_{char} and B^{-2}. This, in turn, supports the validity of eq 9 to relate $\delta_{wet}^{20^\circ C}$ and $\delta_{wet}^{40^\circ C}$. It must be emphasized that the effect on D is still more decisive, since it results opposite to the expected behavior of the thermally activated diffusional process.

The fact that a grafted PNIPAM brush builds a barrier to molecular diffusion, irrespective of its conformational state, is particularly relevant in the design of certain thermally nanoactuated ion gating.[9]

4. CONCLUSIONS

A number of open questions related to thin grafted PNIPAM brushes with varying grafting density were thoroughly discussed on the basis of an electrochemical characterization strategy. In particular, answers were given for individual effects of the thermally induced collapse transition on both molecular transport through the brush and blocking character of the modified surface, respectively. In addition, further insight into the transport behavior of brushes synthesized from SAM monolayers was gained, and consequently, some clarity was brought to otherwise unanswered aspects of earlier findings. A quantitative description of mass transport processes through the PNIPAM brushes could be achieved thanks to the use of impedance spectroscopy. We were able to describe how conformational changes due to the thermal collapse of the PNIPAM brush influence transport properties.

More specifically, we have shown the following:

(1) When the brush is absent or it has been grown from an initial SAM with a low concentration of the initiator thiol (5%), a semi-infinite diffusion limiting step takes place in the electrolyte, while the charge transfer step remains also unaffected by the brush.

(2) In thin brushes, reaction sites on the surface are given by hydrophilic regions or defects on the initial SAM that determine the active area of the electrode. The fractional surface coverage does not vary with the polymer brush conformational changes. This behavior is related only to thin brushes.

(3) Characteristic features of the voltammetric responses, for example, peaks separation and sharpness, may be used to confirm results obtained by impedance spectroscopy. However, obtaining a fit parameter like B that is independent of A_e represents a considerable advantage of impedance spectroscopy over other electrochemical techniques in calculating the diffusion coefficient.

(4) The calculated fractional coverage and other calculated microscopic variables are in agreement with comparable literature data. This validates the proposed impedance theoretical model. According to this model, it is possible to separate individual effects of the thermally induced collapse transition on both molecular transport through the brush and blocking character of the modified surface, respectively.

(5) Grafted PNIPAM brushes grown from an initial SAM containing a concentration of thiol initiator ≥25% sets up a barrier to molecular diffusion irrespective of its conformational state. An additional hindrance to diffusion is associated with the brush collapse.

■ ASSOCIATED CONTENT

Supporting Information

AFM images in lateral force mode of the initiating layers corresponding to a SAM obtained with 5% thiol initiator and a SAM with a 100% inert thiol and a discussion of these images in terms of the absence of phase separation domains in the mixed

thiol SAM and equivalent literature data. This material is available free of charge via the Internet at http://pubs.acs.org.

AUTHOR INFORMATION

Corresponding Author

*Tel: +54-221-425-7430. Fax: +54-221-425-4642. E-mail: gervasi@inifta.unlp.edu.ar (C.A.G.) and azzaroni@inifta.unlp.edu.ar (O.A.). Homepage: http://softmatter.quimica.unlp.edu.ar.

Notes

The authors declare no competing financial interest.

ACKNOWLEDGMENTS

This work was financially supported by the Marie Curie project "Transport Studies on Polymer Based Nanodevices and Assemblies for Delivery and Sensing". (TRASNADE) (FP7 People—International Research Staff Exchange Scheme—Grant ref: 247656). C.A.G. gratefully acknowledges the Comisión de Investigaciones Científicas y Técnicas Buenos Aires (CICBA) for his position as a member of the Carrera del Investigador Científico. O.A. is a CONICET fellow and acknowledges financial support from the Alexander von Humbodlt Stiftung (Germany), the Max Planck Society (Germany), and (ANPCyT-Argentina—PICT-PRH 163/08—PICT BICENTENARIO 2010-2554). S.M. acknowledges support from the Spanish Ministry of Science and Innovation (MAT2010-18995).

REFERENCES

(1) Jhon, Y. K.; Bhat, R. R.; Jeong, C.; Rojas, O. J.; Szleifer, I; Genzer, J. *Macromol. Rapid Commun.* **2006**, *27*, 697−701.
(2) Malham, I. B.; Bureau, L. *Langmuir* **2010**, *26*, 4762−4768.
(3) Plunkett, K. N.; Zhu, X.; Moore, J. S.; Leckband, D. E. *Langmuir* **2006**, *22*, 4259−4266.
(4) Goldstein, R. E. J. *Chem. Phys.* **1984**, *80*, 5340−5341.
(5) Luzinov, I.; Minko, S.; Tsukruk, V. V. *Prog. Polym. Sci.* **2004**, *29*, 635−698.
(6) Gil, E. S.; Hudson, S. M. *Prog. Polym. Sci.* **2004**, *29*, 1173−1222.
(7) Cole, M. A.; Voelcker, N .H.; Thissen, H.; Griesser, H. J. *Biomaterials* **2009**, *30*, 1827−1850.
(8) Guo, W.; Xia, H.; Xia, F.; Hou, X.; Cao, L.; Wang, L.; Xue, J.; Zhang, G.; Song, Y.; Zhu, D.; Wang, Y.; Jiang, L. *ChemPhysChem* **2010**, *11*, 859−864.
(9) Yameen, B.; Ali, M.; Neumann, R.; Ensinger, W.; Knoll, W.; Azzaroni, O. *Small* **2009**, *5*, 1287−1291.
(10) Reuber, J.; Reinhardt, H.; Johannsmann, D. *Langmuir* **2006**, *22*, 3362−3367.
(11) Jones, D. M.; Brown, A. A.; Huck, W. T. S. *Langmuir* **2002**, *18*, 1265−1269.
(12) Matyjaszewski, K.; Gaynor, S.; Grezta, D.; Mardare, D.; Shigemoto, T. *J. Phys. Org. Chem.* **1995**, *8*, 306−315.
(13) Matyjaszewski, K.; Patten, T. E.; Xia, J. *J. Am. Chem. Soc.* **1997**, *119*, 674−680.
(14) Press, W. H.; Teukolsky, S. A.; Vetterling, W. T.; Flannery, B. P. *Numerical Recipes in FORTRAN: The Art of Scientific Computing*, 2nd ed.; Cambridge University Press: Cambridge, United Kingdom, 1992.
(15) Liu, X.; Ye, Q.; Yu, B.; Liang, Y.; Liu, W.; Zhou, F. *Langmuir* **2010**, *26*, 12377−12382.
(16) Kaifer, A.; Gómez-Kaifer, M. *Supramolecular Electrochemistry*; Wiley-VCH: Weinheim, Germany, 1999; pp 193−194.
(17) Finklea, H. O. In Electrochemistry of Organized Monolayers of Thiols and Related Molecules on Electrodes. *Electroanalytical Chemistry*; Bard, A. J., Rubinstein, I., Eds.; Marcel Dekker Inc.: New York, 1996; Vol. *19*, pp 160−239.
(18) Janek, R. P.; Fawcett, W. R. *Langmuir* **1998**, *14*, 3011−3018.
(19) Finklea, H. O.; Snider, D. A.; Fedyk, J. *Langmuir* **1993**, *9*, 3660−3667.
(20) Bard, A. J.; Faulkner, R. L. Electrochemical Methods. *Fundamentals and Applications*, 2nd ed.; John Wiley & Sons, Inc.: New York, 2001; pp 236−238.
(21) Zhou, J.; Liu, J.; Wang, G.; Lu, X.; Wen, Z.; Li, J. *Adv. Funct. Mater.* **2007**, *17*, 3377−3382.
(22) Alonso García, T.; Gervasi, C. A.; Rodríguez Presa, M. J.; Irigoyen Otamendi, J.; Moya, S. E.; Azzaroni, O. Manuscript in preparation.
(23) Rodríguez Presa, M. J.; Gassa, L. M.; Azzaroni, O.; Gervasi, C. A. *Anal. Chem.* **2009**, *81*, 7936−7943.
(24) Azzaroni, O.; Gervasi, C. A. In Functional Polymer Films. *Characterization and Applications*, 1st ed.; Knoll, W., Advincula, R. C., Eds.; Wiley-VCH Verlag GmbH & Co. KgaA: Weinheim, Germany, 2011; Vol. *2*, Chapter 26, pp 809−830.
(25) Berry, J.; Norcliffe, A.; Humble, S. *Introductory Mathematics through Science Applications*; Cambridge University Press: New York, 1996; p 57.
(26) Sui, X.; Chen, Q.; Hempenius, M. A.; Vancso, G. J. *Small* **2011**, *7*, 1440−1447.
(27) Kidoaki, S.; Ohya, S.; Nakayama, Y.; Matsuda, T. *Langmuir* **2001**, *17*, 2402−2407.